Knockdown of endoplasmic reticulum chaperone BiP leads to the death of parvocellular AVP/CRH neurons in mice

Yohei Kawaguchi[1], Daisuke Hagiwara[1], Tetsuro Tsumura[1], Takashi Miyata[1], Tomoko Kobayashi[1], Mariko Sugiyama[1], Takeshi Onoue[1], Yoshinori Yasuda[1], Shintaro Iwama[1], Hidetaka Suga[1], Ryoichi Banno[1,2], Valery Grinevich[3], Hiroshi Arima[1]

[1]Department of Endocrinology and Diabetes, Nagoya University Graduate School of Medicine, Nagoya, 466-8550, Japan

[2]Research Center of Health, Physical Fitness and Sports, Nagoya University, Nagoya 464-8601, Japan

[3]Department of Neuropeptide Research in Psychiatry, Central Institute of Mental Health, Medical Faculty Mannheim, University of Heidelberg, 68159 Mannheim, Germany

Correspondence

Daisuke Hagiwara, Department of Endocrinology and Diabetes, Nagoya University Graduate School of Medicine, Nagoya, 466-8550, Japan

Email: d-hagiwara@med.nagoya-u.ac.jp

Hiroshi Arima, Department of Endocrinology and Diabetes, Nagoya University Graduate School of Medicine, Nagoya, 466-8550, Japan

Email: arima105@med.nagoya-u.ac.jp

Abstract

Arginine vasopressin (AVP) is expressed in both magnocellular (magnAVP) and parvocellular AVP (parvAVP) neurons of the paraventricular nucleus, and AVP colocalizes with corticotropin-releasing hormone (CRH) only in the parvocellular neurons. The immunoglobulin heavy chain binding protein (BiP) is a major endoplasmic reticulum (ER) chaperone which regulates the unfolded protein response under ER stress. We previously demonstrated that knockdown of BiP in magnAVP neurons exacerbated ER stress, which resulted in the autophagy-associated cell death of magnAVP neurons. Using the same approach, in the present study we examined the role of BiP in mouse parvAVP/CRH neurons. Our data demonstrate that BiP is expressed in mouse parvAVP/CRH neurons under non-stress conditions and is upregulated in proportion to the increase in CRH expression after adrenalectomy. For BiP knockdown in parvAVP/CRH neurons, we utilized a viral approach in combination with shRNA interference. Knockdown of BiP expression induced ER stress in parvAVP/CRH neurons, as reflected by the expression of C/EBP homologous protein. Furthermore, BiP knockdown led to the loss of parvAVP/CRH neurons after four weeks. In summary, our results demonstrate that BiP plays a pivotal role in parvAVP/CRH neurons, which function as neuroendocrine cells producing a large amount of secretory proteins.

KEYWORDS

corticotropin-releasing hormone, arginine vasopressin, parvocellular neuron, immunoglobulin heavy chain binding protein, endoplasmic reticulum stress

1 INTRODUCTION

Arginine vasopressin (AVP) neurons are classified as magnocellular (magnAVP) and parvocellular AVP (parvAVP) neurons(1). AVP is synthesized in magnAVP neurons in the supraoptic nucleus (SON) and paraventricular nucleus (PVN) of the hypothalamus, and is released from the posterior pituitary into the systemic circulation, where it plays an important role in water balance as an antidiuretic hormone(2). In contrast, AVP that is colocalized with corticotropin-releasing hormone (CRH) in the parvAVP neurons of the PVN reaches corticotrophs in the anterior pituitary through the hypophyseal portal vein(3). AVP stimulates ACTH release in a coordinated manner with CRH(4-10), which has been implicated in a wide range of physiological processes including not only the hypothalamic-pituitary-adrenal (HPA) axis(3), but also feeding behavior(11), autonomic regulation(12, 13), emotional responses(14), and cerebellar plasticity(15). While AVP gene expression in parvAVP neurons is suppressed under normal conditions, it has been shown to be upregulated upon glucocorticoid deprivation(16-20).

Excess synthesis of secretory proteins leads to endoplasmic reticulum (ER) stress in secretory cells(21-23). The unfolded protein response (UPR) triggered by this ER stress induces a variety of cellular reactions as a protective mechanism whereby ER folding capacity is upregulated and protein load is decreased in the ER(24, 25). The immunoglobulin heavy chain binding protein (BiP), also referred to as the 78-kDa glucose-regulated protein (GRP78), is one of the most abundant ER chaperones(26-28). BiP binds to newly synthesized polypeptides for protein folding and to misfolded proteins to facilitate correct refolding and to prevent their aggregation(29). Although BiP is a ubiquitous protein, our previous study demonstrated that *Bip* mRNA is highly expressed in the SON and PVN of the hypothalamus(23). This indicates that BiP expression levels differ between cell types and tissues.

We previously demonstrated that BiP knockdown in magnAVP neurons led to ER stress and activated autophagy followed by magnAVP neuronal loss, suggesting that BiP is essential for the function and

64 survival of magnAVP neurons (30). In the present study, we used a viral approach in combination with
65 shRNA interference to investigate the role of BiP in parvAVP/CRH neurons.
66
67 **2 MATERIALS AND METHODS**
68 **2.1 Animals**
69 C57BL/6J mice were purchased from Chubu Science Materials (Nagoya, Japan). Mice were maintained
70 under controlled conditions (23.0 ± 0.5°C, lights on 09:00 to 21:00); male mice were used in all experiments.
71 All procedures were approved by the Animal Experimentation Committee of the Nagoya University
72 Graduate School of Medicine and performed in accordance with institutional guidelines for animal care and
73 use. A total of 87 mice were used in the present study.
74
75 **2.2 Brain collection for immunohistochemistry**
76 Mice were injected intracerebroventricularly with 30 μg of colchicine (Sigma-Aldrich, St. Louis, MO,
77 USA) following intraperitoneal administration of pentobarbital (20 mg/kg; Kyoritsu Seiyaku, Tokyo,
78 Japan) on a stereotaxic apparatus (Model 900LS; Kopf Instruments, Tujunga, CA, USA) under anesthesia
79 with 1-2% isoflurane (Wako, Osaka, Japan) using an animal anesthetization device (MA-AT210D;
80 Muromachi Kikai, Tokyo, Japan). Twenty-four hours after colchicine injection, mice were deeply
81 anesthetized and transcardially perfused with a cold fixative containing 4% paraformaldehyde (PFA; Wako)
82 in phosphate-buffered saline (PBS), pH 7.4. After fixation, brains were removed and immersed in the same
83 fixative for 24 h at 4°C, then dissected and cut into 50-μm sections on a vibratome (VT1200 S; Leica
84 Microsystems, Wetzlar, Germany).
85
86 **2.3 Antibodies**

The primary antibodies used for immunohistochemistry included: rabbit anti-CRH (1:1000; T-4037; Peninsula Laboratories International, San Carlos, CA, USA), guinea pig anti-CRH (1:800; T-5007; Peninsula Laboratories International), mouse anti-neurophysin (NP) II [AVP-NP; 1:100; PS41; kindly provided by Dr. Harold Gainer, National Institutes of Health (NIH), Bethesda, MD, USA](31, 32), rabbit anti-GRP78/BiP (1:600; ab21685; Abcam, San Diego, CA, USA), chicken anti-GFP (1:10000; ab13970; Abcam), mouse anti-neurophysin I [oxytocin (OT)-NP; 1:100; PS38; a gift from Dr. Harold Gainer] (31, 32), and rabbit anti-C/EBP homologous protein (CHOP; 1:50; sc-575; Santa Cruz Biotechnology, Dallas, TX, USA). The following secondary antibodies were used: Alexa Fluor 405-conjugated goat anti-mouse IgG (H+L) (1:1000; A31553; Invitrogen, San Diego, CA, USA), Alexa Fluor 488-conjugated goat anti-chicken IgY (H+L) (1:1000; A11039; Invitrogen), Alexa Fluor 546-conjugated donkey anti-mouse IgG (H+L) highly cross-adsorbed (1:1000; A10036; Invitrogen), Alexa Fluor 546-conjugated donkey anti-rabbit IgG (H+L) highly cross-adsorbed (1:1000; A10040; Invitrogen), Cy3-conjugated affinipure donkey anti-guinea pig IgG (H+L) (1:500; 706-165-148; Jackson ImmunoResearch, West Grove, PA, USA), Alexa Fluor 647-conjugated donkey anti-mouse IgG (H+L) highly cross-adsorbed (1:1000; A31571; Invitrogen), and Alexa Fluor 647-conjugated donkey anti-rabbit IgG (H+L) highly cross-adsorbed (1:1000; A31573; Invitrogen).

2.4 Immunohistochemistry

Floating brain sections were washed with PBS and 0.3% Triton X-100 (Katayama Chemical Industries, Osaka, Japan) in PBS, followed by blocking with a mixture of 5% normal goat serum and 3% bovine serum albumin in PBS for 1 h at room temperature (RT). For immunofluorescence staining, sections were incubated with primary antibodies overnight at 4℃. After rinsing in PBS with 0.05% Tween 20 (Sigma-Aldrich), sections were treated with corresponding secondary antibodies for 2 h at RT. Fluorescence images

were acquired with a laser-scanning confocal microscope (TiE A1R; Nikon Corporation, Tokyo, Japan) and processed using Adobe Photoshop CS5 (Adobe Systems, San Jose, CA, USA). For the terminal deoxynucleotidyl transferase-mediated dUTP nick end-labeling (TUNEL) assay, the In Situ Cell Death Detection Kit, TMR red (Roche, Basel, Switzerland) was used according to the manufacturer's instructions.

2.5 Adrenalectomy

Two-month-old mice were anesthetized with 1-2% isoflurane (Wako) using an animal anesthetization device (MA-AT210D), and each group of mice underwent bilateral adrenalectomy (ADX) or sham ADX. Both groups of mice were provided 2.5% D-glucose (Wako) and 0.45% NaCl (Sigma-Aldrich) in water with corticosterone (approximately 300 μg/d; Sigma-Aldrich) for three days after surgery, followed by the same water without corticosterone. Two weeks after surgery, each procedure described above was performed for immunohistochemistry or quantitative real-time RT-PCR.

2.6 Quantification of CRH and BiP immunosignal intensity

The best-matched slices for the PVN at 0.82 mm caudal from the bregma in accordance with the mouse brain atlas (33) were selected from each mouse for analyses. Densitometric analyses of immunosignal intensity were performed for CRH expression in the whole PVN and each parvAVP/CRH neuron of the PVN, and BiP expression in each parvAVP/CRH and magnAVP neuron of the PVN. Using NIS-Element Analysis software (Nikon), CRH and BiP immunosignal intensity was measured in the bilateral PVN, and the two bilateral values were averaged to obtain the mean value. The mean values for each mouse were subjected to statistical analyses.

2.7 Quantitative real-time RT-PCR

Mice were sacrificed by cervical dislocation, and brains were immediately dissected followed by PVN isolation. The samples were frozen in liquid nitrogen and stored at −80°C until RNA extraction. Total RNA was extracted using TRIzol (Invitrogen) and the RNeasy kit (QIAGEN, Hilden, Germany). RNA purity was measured using spectrophotometry to ensure 260/280 readings were > 1.8. RNA integrity was assessed by electrophoresis on a 1% agarose gel including formaldehyde (Wako). One microgram of total RNA was reverse transcribed using the ReverTra Ace™ qPCR RT Kit (TOYOBO, Osaka, Japan). Quantitative real-time PCR reactions were performed using Power SYBR Green PCR Master Mix (Applied Biosystems, Waltham, MA, USA). As an internal standard control, *glyceraldehyde 3-phosphate dehydrogenase (Gapdh)* mRNA expression was simultaneously quantified. There were no significant differences in Cq value of *Gapdh* mRNA between each group (sham, 17.71 ± 0.14, ADX, 17.91 ± 0.18, P = .4176, sham vs ADX; vehicle, 18.55 ± 0.10, colchicine, 18.75 ± 0.17, P = .4516, vehicle vs colchicine). The following primer sequences were used: *Crh* mRNA, 5'-ACCAAGGGAGGAGAAGAGAGCG-3' (forward), 5'-GCTGCTCCGGCTGCAAGAAA-3' (reverse); *Bip* mRNA, 5'-GACATTTGCCCCAGAAGAAA-3' (forward), 5'-CTCATGACATTCAGTCCAGCA-3' (reverse); and *Gapdh* mRNA, 5'-AGGTCGGTGTGAACGGATTTG-3' (forward), 5'-TGTAGACCATGTAGTTGAGGTCA-3' (reverse). Relative mRNA expression was calculated using the comparative Cq method, and analyses were performed using the CFX Maestro qPCR system (Bio-Rad, La Jolla, CA, USA). Housekeeping gene stability was assessed for each individual experiment using duplicate reactions. The specificity of amplification was confirmed through analysis of the melt curves in the SYBR Green qPCR assay and separation of the PCR products by electrophoresis.

2.8 Viral vectors

Recombinant adeno-associated viruses (rAAVs; serotype 1/2) carrying a conserved 1.9 kb AVP promoter

followed by Venus cDNA (rAAV-AVPp-Venus), a mouse BiP shRNA cassette (rAAV-AVPp-BiP shRNA) from the Hspa5 mouse shRNA plasmid (TR500881; OriGene, Rockville, MD, USA), or a scrambled shRNA cassette (rAAV-AVPp-scrambled shRNA) were cloned and produced as reported(30, 34, 35). The sequence of the BiP shRNA was: 5'-TTCTACCATAAGTGACACCAATAAATGTT-3'. Genomic titers of the viruses were determined with the QuickTiter AAV Quantitation Kit (Cell Biolabs, San Diego, CA, USA) and RT-PCR using the ABI 7700 cycler (Applied Biosystems). The rAAV titers were between 10^9-10^{10} genomic copies/μl.

2.9 Stereotaxic targeting of rAAVs into the mouse PVN

Two-month-old mice were anesthetized with 1-2% isoflurane (Wako) using an animal anesthetization device (MA-AT210D) and placed on the stereotaxic apparatus (Model 900LS; Kopf Instruments). rAAV injections were performed using glass pipettes prepared from 1-5 μl micropipettes (708707; Brand, Wertheim, Germany) with a glass pipette puller (PC-100; Narishige, Tokyo, Japan) as reported previously(30). The injection volume of the rAAVs was 200 nl per nucleus. The injection coordinates for the whole PVN were A/P −0.8 mm, M/L ±0.25 mm, D/V −4.6 mm in accordance with the mouse brain atlas(33).

2.10 Cell counting

The best-matched sections for the PVN at 0.82 mm caudal from the bregma in accordance with the mouse brain atlas (33) were selected from each mouse for quantification of parvAVP/CRH, OT, and magnAVP neurons. Using NIS-Element Analysis software (Nikon), the number of immunolabeled cells was counted in the bilateral PVN, and the two bilateral counts were averaged to obtain the mean number of cells. The mean values for each mouse were subjected to statistical analyses.

179

180 **2.11 Electron microscopy**

181 Mice were deeply anesthetized and transcardially perfused with 4% PFA (Wako) and 0.1% glutaraldehyde
182 (GA; Wako) in PBS. Brains were then immersed in 4% PFA (Wako) for 24 h at 4℃. After fixation, brains
183 were cut into 100-μm sections on a vibratome (VT1200 S; Leica Microsystems). Free-floating sections
184 were washed with 0.1 M phosphate buffer (PB) and 0.1% Triton X-100 (Katayama Chemical Industries) in
185 PB, followed by incubation with a guinea pig anti-CRH antibody (1:800; T-5007; Peninsula Laboratories
186 International) overnight at 4℃. Sections were then washed with 0.1 M PB and incubated with horse anti-
187 guinea pig IgG (H + L) (1:200; BA-7000; Vector Laboratories, Newark, CA, USA) for 2 h at RT. Sections
188 were washed then treated with avidin-biotin complex solution (1:100; Vectastain ABC-HRP kit; PK-4000;
189 Vector Laboratories) for 90 min at RT. Signals were developed with 0.1 M PB containing 0.1% 3, 3'-
190 diaminobenzidine dihydrochloride (Sigma-Aldrich) and 0.004% hydrogen peroxide (Wako). The stained
191 sections were further fixed in 2.5% GA (Wako) in 0.1 M PB overnight at 4℃, followed by post-fixation
192 with 2% osmium tetroxide (Electron Microscopy Sciences, Hatfield, UK) for 20 min at 4℃. Each section
193 was dehydrated in a graded ethanol series, treated with propylene oxide (Wako), and embedded in epoxy
194 resin (TAAB 812 resin; TAAB Laboratories Equipment, Aldemaston, UK). The resin was polymerized for
195 48 h at 60℃. Ultrathin sections (70-nm thickness) including the PVN were prepared using an
196 ultramicrotome (EM UC7i; Leica Microsystems) with a diamond knife (Reichert Ultracut S; Leica
197 Microsystems) and counterstained with lead citrate before analysis with an electron microscope (JEM-
198 1400PLUS; JEOL, Tokyo, Japan).

199

200 **2.12 Measurements of plasma corticosterone**

201 Blood was collected via submandibular bleeding from mice and immediately centrifuged for plasma

separation. For restraint stress, mice were confined in a 50 ml plastic tube for 3 h prior to blood collection. Plasma corticosterone was measured using a Corticosterone AssayMax™ ELISA Kit (EC3001-1; AssayPro, St. Charles, MO, USA).

2.13 Statistical analyses

Statistically significant differences between groups were analyzed by either an unpaired Student's two-tailed *t*-test or a one-way ANOVA with repeated measures followed by a Bonferroni post-hoc test, as appropriate. Results are expressed as the mean ± standard error of the mean (SEM), and differences were considered statistically significant at a value of $P < .05$.

3 RESULTS

3.1 BiP expression in CRH neurons in the mouse PVN

We first examined BiP expression in parvAVP neurons in the mouse PVN. Immunohistochemistry for CRH, AVP, and BiP revealed that BiP was expressed in CRH neurons in the PVN (Figure 1A). Furthermore, BiP immunostaining in CRH neurons ($P = .0003$, sham vs ADX; Figure 1B, C) and *Bip* mRNA expression in the PVN (Figure 1D) were increased following ADX ($P = .0435$, sham vs ADX).

3.2 Validation of rAAV vectors in CRH neurons in the mouse PVN

Next, we validated the effectiveness of our rAAV vectors harboring an AVP promoter in CRH neurons in the mouse PVN (Figure 2). 95.0% of CRH-immunoreactive (ir) cells (parvAVP neurons, 642/676 cells) and 98.2% of AVP-ir cells (including magnAVP neurons and a subset of parvAVP neurons, 552/562 cells) expressed Venus (Figure 2B). Also, 51.5% and 44.3% of Venus-ir cells (642/1246 and 552/1246 cells) were CRH-positive (parvAVP neurons) and AVP-positive (including magnAVP neurons and a subset of parvAVP

neurons), respectively (Figure 2B). Since 7.0% of CRH-ir cells (47/676 cells) were AVP-positive, the proportion of CRH or AVP-ir cells (including magnAVP and parvAVP neurons) among the Venus-ir cells was 92.1% (1147/1246 cells; Figure 2B). In contrast, only 1.7% of Venus-ir cells (15/861 cells) were OT-positive, and 11 out of the 15 OT-positive cells also expressed AVP.

Two weeks after rAAV-AVPp-Venus injection into the PVN, 95.0% of CRH-ir cells (642/676 cells) expressed Venus, while only 7.0% of CRH-ir cells (47/676 cells) were AVP-positive. We then compared the proportion of AVP and Venus-ir cells to CRH neurons in rAAV-AVPp-Venus injected mice with and without ADX (Figure S1). ADX significantly increased the number of CRH-ir cells (P = .0007, sham vs ADX; Figure S1B) and the proportion of AVP-ir cells to CRH-ir cells in the PVN (sham, 7.0%, 47/676 cells; ADX, 38.8%, 266/686 cells; P < .0001, sham vs ADX; Figure S1C); however, the proportion of Venus-ir cells to CRH-ir cells after ADX was comparable to that in the sham group (sham, 95.0%, 642/676 cells; ADX, 96.9%, 664/686 cells; P = .2841, sham vs ADX; Figure S1C).

3.3 BiP knockdown in CRH neurons leads to their loss

We injected rAAV-AVPp-BiP shRNA into the bilateral PVN for BiP knockdown in CRH neurons and rAAV-AVPp-scrambled shRNA as a control (Figure 3). BiP expression was decreased to 45.9% in CRH neurons two weeks after injection of rAAV-AVPp-BiP shRNA (P = .0007, cont sh 2wk vs BiP sh 2wk; Figure 3B).

To examine the effects of BiP knockdown on CRH neuronal viability, we counted CRH neurons in the PVN injected with rAAV-AVPp-BiP shRNA or rAAV-AVPp-scrambled shRNA as well as in un-injected mice (Figure 4A.B). There were no significant differences in the number of CRH neurons between the un-injected and scrambled shRNA groups ($F_{4,10}$ = 18.23, P = 1.00; Figure 4B). In contrast, while mice injected with rAAV-AVPp-BiP shRNA presented no significant changes two weeks after injection ($F_{4,10}$ = 18.23, P = 1.00), CRH neurons were significantly decreased to approximately 70% of control at both four and twelve

248 weeks after BiP shRNA injection (BiP sh 4wk, $F_{4,10} = 18.23$, $P < .001$; BiP sh 12wk, $F_{4,10} = 14.92$, $P < .001$;
249 Figure 4B). In contrast to CRH neurons, there were no significant changes in the number of OT neurons
250 after rAAV-AVPp-BiP shRNA injection into the PVN ($F_{3,8} = 3.66$, $P = .780$; Figure S2).
251
252 **3.4 BiP knockdown in CRH neurons leads to ER stress and autophagy**
253 Immunohistochemistry for the ER stress marker CHOP revealed that CHOP-expressing CRH neurons were
254 significantly increased in the PVN two weeks after the injection of rAAV-AVPp-BiP shRNA at a time point
255 when CRH neurons were not yet lost ($P = .0274$, cont sh 2wk vs BiP sh 2wk; Figure 5). To investigate
256 whether apoptosis is involved in CRH neuronal loss by BiP knockdown, we performed a TUNEL assay.
257 There were almost no TUNEL-positive cells four weeks after either rAAV-AVPp-BiP shRNA or rAAV-
258 AVPp-scrambled shRNA injection (Figure S3). Immunoelectron microscopic analyses of CRH neurons
259 revealed conspicuous autophagic vacuoles in CRH neurons of the PVN two weeks after BiP shRNA
260 injection (Figure 4C). Furthermore, relatively well-preserved nuclear structure and large vacuoles
261 containing various organelles undergoing degradation were present in CRH neurons four weeks after BiP
262 knockdown, while no obvious micromorphological changes were observed in CRH neurons of control mice
263 (Figure 4C).
264
265 **3.5 The HPA response is maintained after BiP knockdown in CRH neurons**
266 There were no changes in CRH expression in the PVN of mice injected with rAAV-AVPp-BiP shRNA or
267 rAAV-AVPp-scrambled shRNA at twelve weeks post-injection when approximately 30% of CRH neurons
268 had been lost ($P = .4178$, cont sh 12wk vs BiP sh 12wk; Figure S4A). In addition, there were no significant
269 differences in plasma corticosterone levels under normal conditions and after restraint stress in mice

injected with rAAV-AVPp-BiP shRNA or scrambled shRNA at twelve weeks post-injection (naive, P = .7039, cont sh 12wk vs BiP sh 12wk; restraint, P = .6540, cont sh 12wk vs BiP sh 12wk; Figure S4B).

3.6 BiP knockdown in magnAVP neurons induces ER stress leading to loss of magnAVP neurons

BiP expression was decreased to 67.2% in magnAVP neurons two weeks after injection of rAAV-AVPp-BiP shRNA into the PVN (P = .0458, cont sh 2wk vs BiP sh 2wk; Figure S5). The number of magnAVP neurons was decreased to approximately 50% at both four and twelve weeks after virus injection (BiP sh 4wk, $F_{4,10} = 43.87$, $P < .001$; BiP sh 12wk, $F_{4,10} = 43.87$, $P < .001$; Figure S6). CHOP-expressing magnAVP neurons were significantly increased in the PVN two weeks after injection with rAAV-AVPp-BiP shRNA at a time point when CRH neurons were not yet lost (P = .0044, cont sh 2wk vs BiP sh 2wk; Figure S7).

4 DISCUSSION

In the present study, we demonstrated that the ER chaperone BiP was expressed in parvAVP/CRH neurons in the mouse PVN, and that it was upregulated in proportion to the increase in CRH expression after ADX. Moreover, we revealed that BiP knockdown in CRH neurons induced ER stress followed by CRH neuronal loss in the PVN.

We previously reported that (1) BiP is expressed in AVP neurons of the SON and PVN, (2) it is upregulated by dehydration, and (3) BiP knockdown in AVP neurons of the SON and PVN leads to ER stress and loss of AVP neurons(30). In the current study, we distinguished parvAVP/CRH neurons from magnAVP neurons by CRH immunostaining and investigated BiP expression and the effect of BiP knockdown on magnAVP and parvAVP/CRH neurons separately. Our data revealed that BiP was expressed in parvAVP/CRH as well as magnAVP neurons without ADX. Since CRH immunostaining does not work well in mice without colchicine treatment(36), we performed an intracerebroventricular injection of

293 colchicine, which could cause various types of cellular stress in neurons. Indeed, *Bip* and *Crh* mRNA
294 expression in the PVN was increased after colchicine treatment (Figure S8). On the other hand, we
295 previously demonstrated that the distribution of *Bip* mRNA overlaps that of *Crh* mRNA in the PVN by in
296 situ hybridization without colchicine treatment(23), indicating that BiP is expressed in parvAVP/CRH
297 neurons even under normal conditions. Furthermore, our data also demonstrated that BiP expression in
298 parvAVP/CRH neurons increased in proportion to CRH upregulation following ADX. These data suggest
299 that BiP is required for the characteristic production of a large amount of secretory proteins in both
300 magnAVP and parvAVP/CRH neurons and thus their function as neuroendocrine cells, and that the demand
301 for BiP is increased in proportion to secretory proteins in each neuron system.

302 Unresolved ER stress and a prolonged UPR are known to induce apoptosis(37). Indeed, apoptosis was
303 reported to be involved in the death of the inner cell mass of embryonic BiP whole-body knockout mice(38),
304 as well as in hepatocytes(39), myocytes(40), respiratory epithelial cells(41, 42), hematopoietic cells(43),
305 Purkinje cells(44), oligodendrocytes, and Schwann cells(45) in corresponding BiP conditional knockout
306 studies, mainly based on TUNEL assay results. In the present study, however, we observed no increase in
307 TUNEL-positive cells in the PVN nor micromorphological features characteristic of apoptosis in CRH
308 neurons even though CRH neurons were dying after BiP knockdown. Furthermore, autophagic vacuoles
309 were increased two weeks after BiP knockdown, and large vacuoles containing various organelles
310 undergoing degradation were presented in CRH neurons four weeks after BiP knockdown. This is consistent
311 with our previous study demonstrating that autophagy-associated cell death is involved in magnAVP
312 neuronal loss after BiP knockdown(30).

313 The effects of BiP knockout/knockdown on cell viability vary between cell types and tissues(46). In the
314 present study, BiP knockdown in parvAVP/CRH neurons resulted in the loss of approximately 30% of
315 parvAVP/CRH neurons. In contrast, we previously demonstrated that BiP knockdown in magnAVP neurons

induced the death of approximately 90% of magnAVP neurons(30). These differences in cell death ratios might be explained by the difference in the amount of protein synthesized within the cells. It should be also mentioned that BiP knockdown efficiency in parvAVP/CRH and magnAVP neurons using our AVP neuron-specific BiP shRNA methods was approximately 50%. More cell death in parvAVP/CRH neurons could be induced by using more efficient BiP knockdown system operating a CRH promoter, which is predominantly active in this particular cell type under basal and acute stress conditions(47, 48).

In the present study, there were no significant changes in CRH expression in the PVN between control and BiP knockdown mice twelve weeks after BiP knockdown at a time point when approximately 30% of CRH neurons have been lost. Furthermore, there were no differences in plasma corticosterone levels between control and BiP knockdown mice. These results suggest that residual CRH neurons might compensate for CRH neuronal loss due to BiP knockdown.

In parvAVP/CRH neurons, AVP is suppressed under normal conditions and upregulated under stress conditions such as adrenal insufficiency(19, 49) and inflammation(50); however, whether all CRH neurons in the PVN potentially express AVP or not remains to be elucidated. In the current study, 95% of CRH neurons were Venus-positive in the PVN of mice injected with rAAV-AVPp-Venus, whereas only 7.0% of CRH neurons were AVP-positive. The discrepancy in expression between AVP and Venus in CRH neurons might be attributed to Venus being more stable and detectable compared to AVP. These results also suggest that almost all CRH neurons in the PVN could express AVP.

In the current study, we needed colchicine treatment to effectively stain for CRH, which resulted in increases in *Bip* mRNA in the PVN. Thus, colchicine treatment itself increased ER stress in CRH neurons, which is a limitation of this study.

In conclusion, the current study revealed that the expression of BiP (an ER chaperone) in parvAVP/CRH neurons is upregulated in response to increased CRH synthesis following ADX. Furthermore, BiP

knockdown in parvAVP/CRH neurons induced ER stress and cell death in CRH neurons. Taken together, these results demonstrate that BiP has an essential role in the survival of parvAVP/CRH neurons.

ACKNOWLEDGEMENTS

We thank Judith Müller for packaging the viral vectors and Michiko Yamada, Mayu Sakakibara, and Mika Soen for their helpful technical assistance. This work was supported by JSPS KAKENHI Grant Number 21K20930 (to Y.K.), JSPS KAKENHI Grant Number 15K19530 and 21K08552 (to D.H.), an Alexander von Humboldt Foundation Research Fellowship (to D.H.), JSPS KAKENHI Grant Number 17K09878 (to H.S.), the Acceleration Program for Intractable Diseases Research utilizing Disease-specific iPS cells of the Research Center Network for Realization of Regenerative Medicine from the Japan Agency for Medical Research and Development (to H.S.), Nagoya University Hospital Funding for Clinical Research (to H.S.), and the Suzuken Memorial Foundation (to H.A.).

CONFLICT OF INTEREST

The authors declare that they have no conflict of interest.

AUTHOR CONTRIBUTIONS

Yohei Kawaguchi: Methodology, Validation, Formal analysis, Investigation, Data Curation, Writing – original draft, Writing – review and editing, Visualization, Funding acquisition. **Daisuke Hagiwara:** Conceptualization, Methodology, Formal analysis, Data curation, Writing - original draft, Writing - review and editing, Visualization, Supervision, Project administration, Funding acquisition. **Tetsuro Tsumura:** Formal analysis, Methodology, Data curation. **Takashi Miyata:** Formal analysis, Methodology, Data curation. **Tomoko Kobayashi:** Methodology, Data curation. **Mariko Sugiyama:** Methodology, Data

curation. **Takeshi Onoue:** Methodology, Data curation. **Yoshinori Yasuda:** Methodology, Data curation. **Shintaro Iwama:** Methodology, Data curation. **Hidetaka Suga:** Methodology, Data curation, Funding acquisition. **Ryoichi Banno:** Methodology, Data curation. **Valery Grinevich:** Methodology, Resources. **Hiroshi Arima:** Conceptualization, Writing - original draft, Writing - review and editing, Supervision, Project administration, Funding acquisition. All of the authors read and approved the final version of the manuscript for submission.

DATA AVAILABILITY

All data generated in this study will be available from the corresponding author upon request.

Figure legends

FIGURE 1 BiP expression in CRH and magnAVP neurons of the mouse PVN. (A) Representative images of immunofluorescence staining for CRH (green), AVP (cyan), and BiP (red) in the mouse PVN. Higher magnification images of the boxed areas including representative cells are shown in the insets at the upper left. The arrows and arrowheads indicate CRH and magnAVP neurons, respectively. Scale bar: 100 μm. (B) Representative images of immunofluorescence staining for CRH (green) and BiP (red) in the mouse PVN in the sham and ADX groups. Higher magnification images of the boxed areas including representative cells are shown in the insets at the upper left. The arrows indicate CRH neurons. Scale bar: 100 μm. (C) CRH and BiP expression levels per CRH neuron of the PVN in the sham and ADX groups. Mean CRH and BiP expression levels in the sham group are expressed as 100. Results were analyzed by an unpaired Student's *t*-test and are expressed as mean ± SEM (n = 3 per group). (D) Quantitative real-time RT-PCR analysis for *Crh* and *Bip* mRNA in the PVN in the sham and ADX groups. Mean mRNA expression levels in the sham group are expressed as 100. Results were analyzed by an unpaired Student's two-tailed

385 *t*-test and are expressed as mean ± SEM (n = 7 per group).

386

387 **FIGURE 2.** Validation of rAAV vectors in the mouse PVN. (A) Representative images of
388 immunofluorescence staining to detect CRH (red) and AVP (cyan) neurons, and to enhance the Venus signal
389 (green) in the PVN two weeks after rAAV-AVPp-Venus injection. Higher magnification images of the boxed
390 areas including representative cells are shown in the insets at the upper left. The arrows and arrowheads
391 indicate CRH and magnAVP neurons, respectively. Scale bar: 100 μm. (B) The proportion of Venus-ir cells
392 in CRH-ir (CRH^+Venus^+/CRH^+, white bar) and AVP-ir cells (AVP^+Venus^+/AVP^+, light gray bar), and that
393 of CRH-ir ($CRH^+Venus^+/Venus^+$, gray bar), AVP-ir ($AVP^+Venus^+/Venus^+$, dark gray bar), and CRH or AVP-
394 ir cells (CRH or $AVP^+Venus^+/Venus^+$, black bar) to Venus-ir cells in the PVN two weeks after rAAV-AVPp-
395 Venus injection.

396

397 **FIGURE 3.** BiP knockdown in mouse CRH neurons. (A) Representative images of immunofluorescence
398 staining for CRH (green) and BiP (red) in the PVN two weeks after injection of rAAV-AVPp-scrambled
399 shRNA (cont sh 2wk) and rAAV-AVPp-BiP shRNA (BiP sh 2wk). Higher magnification images of the
400 boxed areas including representative cells are shown in the insets at the upper left. The arrows indicate
401 CRH neurons. Scale bar: 100 μm. (B) BiP expression levels per CRH neuron of the PVN in the cont sh 2wk
402 and BiP sh 2wk groups. Mean BiP expression levels in the cont sh 2wk group are expressed as 100. Results
403 were analyzed by an unpaired Student's two-tailed *t*-test and are expressed as mean ± SEM (n = 3 per
404 group).

405

406 **FIGURE 4.** CRH neuronal loss after BiP knockdown in the mouse PVN. (A) Representative images of
407 immunofluorescence staining for CRH in the PVN of un-injected mice (no injection), or twelve weeks after

injection of rAAV-AVPp-scrambled shRNA (cont sh 12wk), and at two (BiP sh 2wk), four (BiP sh 4wk), and twelve weeks after rAAV-AVPp-BiP shRNA injection (BiP sh 12wk). Scale bars: 100 μm. (B) The number of CRH neurons in the PVN in the no injection, cont sh 12wk, BiP sh 2wk, BiP sh 4wk, and BiP sh 12wk groups. Results were analyzed by one-way ANOVA followed by a Bonferroni test and are expressed as mean ± SEM (n = 3 per group). (C) Representative immunoelectron microscopic images of CRH neurons in the PVN at two and four weeks after injection of rAAV-AVPp-scrambled shRNA (cont sh 2wk and 4wk) and rAAV-AVPp-BiP shRNA (BiP sh 2wk and 4wk). The arrows indicate autophagic vacuoles. Scale bars: 2 μm.

FIGURE 5. BiP knockdown induced ER stress in CRH neurons. (A) Representative images of immunofluorescence staining for CRH (green) and CHOP (red) in the PVN two weeks after injection of rAAV-AVPp-scrambled shRNA (cont sh 2wk) and rAAV-AVPp-BiP shRNA (BiP sh 2wk). The arrows indicate CRH neurons expressing CHOP. Scale bar: 100 μm. (B) The number of CHOP-ir neurons in CRH neurons of the PVN in the cont sh 2wk and BiP sh 2wk groups. Results are expressed per 100 CRH neurons and analyzed by an unpaired Student's two-tailed t-test and are expressed as mean ± SEM (n = 3 per group).

FIGURE S1. ADX increased AVP expression in CRH neurons in the mouse PVN. (A) Representative images of immunofluorescence staining to detect AVP (cyan) and CRH (red), and to enhance the Venus signal (green) in the PVN two weeks after ADX. Higher magnification images of the boxed areas including representative cells are shown in the insets at the upper left. The arrows indicate CRH neurons. Scale bar: 100 μm. (B) The number of CRH-ir cells in the PVN in the sham and ADX groups. Results were analyzed by an unpaired Student's two-tailed t-test and are expressed as mean ± SEM (n = 3 per group). (C) The proportion of AVP-ir (AVP^+CRH^+/CRH^+) and Venus-ir cells ($Venus^+CRH^+/CRH^+$) relative to CRH-ir cells

in the sham and ADX groups. Results were analyzed by an unpaired Student's two-tailed *t*-test and are expressed as mean ± SEM (*n* = 3 per group).

FIGURE S2. OT neurons after BiP knockdown in AVP neurons in the mouse PVN. (A) Representative images of immunofluorescence staining for OT in the PVN of un-injected mice (no injection), or twelve weeks after injection of rAAV-AVPp-scrambled shRNA (cont sh 12wk), and at four (BiP sh 4wk) and twelve weeks after rAAV-AVPp-BiP shRNA injection (BiP sh 12wk). Scale bars: 100 μm. (B) The number of OT neurons in the PVN in the no injection, cont sh 12wk, BiP sh 4wk, and BiP sh 12wk groups. Results were analyzed by a one-way ANOVA test and are expressed as mean ± SEM (*n* = 3 per group).

FIGURE S3. Evaluation of apoptosis in the mouse PVN after BiP knockdown. Representative TUNEL assay images from the PVN four weeks after injection of rAAV-AVPp-scrambled shRNA (cont sh 4wk) or rAAV-AVPp-BiP shRNA (BiP sh 4wk); some sections were treated with DNase I according to the manufacturer's instructions as positive controls (positive control). 3V, third ventricle; scale bars: 100 μm.

FIGURE S4. The HPA response after BiP knockdown in CRH neurons in the mouse PVN. (A) CRH expression levels in the PVN twelve weeks after injection of rAAV-AVPp-scrambled shRNA (cont sh 12wk) and rAAV-AVPp-BiP shRNA (BiP sh 12wk). Mean CRH expression levels in the cont sh 12wk group are expressed as 100. Results were analyzed by an unpaired Student's two-tailed *t*-test and are expressed as mean ± SEM (*n* = 3 per group). (B) Plasma corticosterone levels under normal conditions (naive) and restraint stress (restraint) in the cont sh 12wk and BiP sh 12wk groups. Results were analyzed by an unpaired Student's two-tailed *t*-test and are expressed as mean ± SEM (*n* = 3 per group).

FIGURE S5. BiP knockdown in mouse magnAVP neurons. (A) Representative images of immunofluorescence staining for AVP (green), CRH (cyan), and BiP (red) in the PVN two weeks after injection of rAAV-AVPp-scrambled shRNA (cont sh 2wk) and rAAV-AVPp-BiP shRNA (BiP sh 2wk). Higher magnification images of the boxed areas including representative cells are shown in the insets at the upper left. The arrows indicate magnAVP neurons. Scale bars: 100 μm. (B) BiP expression levels per magnAVP neuron of the PVN in the cont sh 2wk and BiP sh 2wk groups. Mean BiP expression levels in the cont sh 2wk group are expressed as 100. Results were analyzed by an unpaired Student's two-tailed *t*-test and are expressed as mean ± SEM (n = 3 per group).

FIGURE S6. MagnAVP neuron loss after BiP knockdown in the mouse PVN. (A) Representative images of immunofluorescence staining for AVP and CRH in the PVN of un-injected mice (no injection), or twelve weeks after injection of rAAV-AVPp-scrambled shRNA (cont sh 12wk), and at two (BiP sh 2wk), four (BiP sh 4wk), and twelve weeks after rAAV-AVPp-BiP shRNA injection (BiP sh 12wk). Scale bars: 100 μm. (B) The number of magnAVP neurons in the PVN in the no injection, cont sh 12wk, BiP sh 2wk, BiP sh 4wk, and BiP sh 12wk groups. Results were analyzed by a one-way ANOVA followed by a Bonferroni test and are expressed as mean ± SEM (n = 3 per group).

FIGURE S7. BiP knockdown induced ER stress in magnAVP neurons. (A) Representative images of immunofluorescence staining for AVP (green), CRH (cyan), and CHOP (red) in the PVN two weeks after injection of rAAV-AVPp-scrambled shRNA (cont sh 2wk) and rAAV-AVPp-BiP shRNA (BiP sh 2wk). The arrows indicate magnAVP neurons expressing CHOP. Scale bars: 100 μm. (B) The number of CHOP-ir neurons in magnAVP neurons of the PVN in the cont sh 2wk and BiP sh 2wk groups. Results are expressed

per 100 magnAVP neurons and analyzed by an unpaired Student's two-tailed *t*-test and are expressed as mean ± SEM (*n* = 3 per group).

FIGURE S8. The effects of colchicine intracerebroventricular injection on *Crh* and *Bip* mRNA in the PVN. Quantitative real-time RT-PCR analysis for *Crh* (A) and *Bip* mRNA (B) in the PVN of mice intracerebroventricularly injected with vehicle (vehicle) or colchicine (colchicine). Mean mRNA expression levels in the vehicle group are expressed as 100. Results were analyzed by an unpaired Student's two-tailed *t*-test and are expressed as mean ± SEM (*n* = 7 per group).

REFERENCES

1. Hatton GI. Emerging concepts of structure-function dynamics in adult brain: the hypothalamo-neurohypophysial system. *Prog Neurobiol*. 1990; **34**(6): 437-504.
2. Bisset GW, Chowdrey HS. Control of release of vasopressin by neuroendocrine reflexes. *Q J Exp Physiol*. 1988; **73**(6): 811-72.
3. Vale W, Spiess J, Rivier C, Rivier J. Characterization of a 41-residue ovine hypothalamic peptide that stimulates secretion of corticotropin and beta-endorphin. *Science*. 1981; **213**(4514): 1394-7.
4. Fischman AJ, Moldow RL. In vivo potentiation of corticotropin releasing factor activity by vasopressin analogues. *Life Sci*. 1984; **35**(12): 1311-9.
5. Gillies GE, Linton EA, Lowry PJ. Corticotropin releasing activity of the new CRF is potentiated several times by vasopressin. *Nature*. 1982; **299**(5881): 355-7.
6. Hashimoto K, Murakami K, Hattori T, Ota Z. Synergistic interaction of corticotropin releasing factor and arginine vasopressin on adrenocorticotropin and cortisol secretion in Macaca fuscata. *Acta Med Okayama*. 1984; **38**(3): 261-7.
7. Liu JH, Muse K, Contreras P et al. Augmentation of ACTH-releasing activity of synthetic corticotropin releasing factor (CRF) by vasopressin in women. *J Clin Endocrinol Metab*. 1983; **57**(5): 1087-9.
8. Murakami K, Hashimoto K, Ota Z. Interaction of synthetic ovine corticotropin releasing factor and arginine vasopressin on in vitro ACTH release by the anterior pituitary of rats. *Neuroendocrinology*. 1984; **39**(1): 49-53.
9. Rivier C, Vale W. Interaction of corticotropin-releasing factor and arginine vasopressin on adrenocorticotropin secretion in vivo. *Endocrinology*. 1983; **113**(3): 939-42.
10. Vale W, Vaughan J, Smith M, Yamamoto G, Rivier J, Rivier C. Effects of synthetic ovine corticotropin-releasing factor, glucocorticoids, catecholamines, neurohypophysial peptides, and other substances on cultured corticotropic cells. *Endocrinology*. 1983; **113**(3): 1121-31.
11. Zorrilla EP, Reinhardt LE, Valdez GR et al. Human urocortin 2, a corticotropin-releasing factor (CRF)2 agonist, and ovine CRF, a CRF1 agonist, differentially alter feeding and motor activity. *J Pharmacol Exp Ther*. 2004; **310**(3): 1027-34.
12. Kovacs KJ. CRH: the link between hormonal-, metabolic- and behavioral responses to stress. *J Chem Neuroanat*. 2013; **54**25-33.
13. Wood SK, McFadden K, Griffin T, Wolfe JH, Zderic S, Valentino RJ. A corticotropin-releasing factor receptor antagonist improves urodynamic dysfunction produced by social stress or

partial bladder outlet obstruction in male rats. *Am J Physiol Regul Integr Comp Physiol*. 2013; **304**(11): R940-50.

14. Wang XD, Labermaier C, Holsboer F et al. Early-life stress-induced anxiety-related behavior in adult mice partially requires forebrain corticotropin-releasing hormone receptor 1. *Eur J Neurosci*. 2012; **36**(3): 2360-7.

15. Ito M. Functional roles of neuropeptides in cerebellar circuits. *Neuroscience*. 2009; **162**(3): 666-72.

16. Itoi K, Mouri T, Takahashi K et al. Suppression by glucocorticoid of the immunoreactivity of corticotropin-releasing factor and vasopressin in the paraventricular nucleus of rat hypothalamus. *Neurosci Lett*. 1987; **73**(3): 231-6.

17. Kiss JZ, Mezey E, Skirboll L. Corticotropin-releasing factor-immunoreactive neurons of the paraventricular nucleus become vasopressin positive after adrenalectomy. *Proc Natl Acad Sci U S A*. 1984; **81**(6): 1854-8.

18. Itoi K, Talukder AH, Fuse T et al. Visualization of corticotropin-releasing factor neurons by fluorescent proteins in the mouse brain and characterization of labeled neurons in the paraventricular nucleus of the hypothalamus. *Endocrinology*. 2014; **155**(10): 4054-60.

19. Helmreich DL, Itoi K, Lopez-Figueroa MO, Akil H, Watson SJ. Norepinephrine-induced CRH and AVP gene transcription within the hypothalamus: differential regulation by corticosterone. *Brain Res Mol Brain Res*. 2001; **88**(1-2): 62-73.

20. Sawchenko PE, Swanson LW, Vale WW. Co-expression of corticotropin-releasing factor and vasopressin immunoreactivity in parvocellular neurosecretory neurons of the adrenalectomized rat. *Proc Natl Acad Sci U S A*. 1984; **81**(6): 1883-7.

21. Wiest DL, Burkhardt JK, Hester S, Hortsch M, Meyer DI, Argon Y. Membrane biogenesis during B cell differentiation: most endoplasmic reticulum proteins are expressed coordinately. *J Cell Biol*. 1990; **110**(5): 1501-11.

22. Lipson KL, Fonseca SG, Ishigaki S et al. Regulation of insulin biosynthesis in pancreatic beta cells by an endoplasmic reticulum-resident protein kinase IRE1. *Cell Metab*. 2006; **4**(3): 245-54.

23. Hagiwara D, Arima H, Morishita Y et al. BiP mRNA expression is upregulated by dehydration in vasopressin neurons in the hypothalamus in mice. *Peptides*. 2012; **33**(2): 346-50.

24. Yamamoto K, Sato T, Matsui T et al. Transcriptional induction of mammalian ER quality control proteins is mediated by single or combined action of ATF6alpha and XBP1. *Dev Cell*. 2007; **13**(3): 365-76.

25. Harding HP, Zhang Y, Bertolotti A, Zeng H, Ron D. Perk is essential for translational regulation and cell survival during the unfolded protein response. *Mol Cell*. 2000; **5**(5): 897-904.

26. Haas IG, Wabl M. Immunoglobulin heavy chain binding protein. *Nature*. 1983; **306**(5941): 387-9.
27. Bole DG, Hendershot LM, Kearney JF. Posttranslational association of immunoglobulin heavy chain binding protein with nascent heavy chains in nonsecreting and secreting hybridomas. *J Cell Biol*. 1986; **102**(5): 1558-66.
28. Munro S, Pelham HR. An Hsp70-like protein in the ER: identity with the 78 kd glucose-regulated protein and immunoglobulin heavy chain binding protein. *Cell*. 1986; **46**(2): 291-300.
29. Gething MJ. Role and regulation of the ER chaperone BiP. *Semin Cell Dev Biol*. 1999; **10**(5): 465-72.
30. Kawaguchi Y, Hagiwara D, Miyata T et al. Endoplasmic reticulum chaperone BiP/GRP78 knockdown leads to autophagy and cell death of arginine vasopressin neurons in mice. *Sci Rep*. 2020; **10**(1): 19730.
31. Ben-Barak Y, Russell JT, Whitnall M, Ozato K, Gainer H. Phylogenetic cross-reactivities of monoclonal antibodies produced against rat neurophysin. *Cell Mol Neurobiol*. 1984; **4**(4): 339-49.
32. Ben-Barak Y, Russell JT, Whitnall MH, Ozato K, Gainer H. Neurophysin in the hypothalamo-neurohypophysial system. I. Production and characterization of monoclonal antibodies. *J Neurosci*. 1985; **5**(1): 81-97.
33. Paxinos G, Franklin KBJ. *The Mouse Brain in Stereotaxic Coordinates* San Diego, Calif. London: Academic, 2001.
34. Schatz KC, Brown LM, Barrett AR, Roth LC, Grinevich V, Paul MJ. Viral rescue of magnocellular vasopressin cells in adolescent Brattleboro rats ameliorates diabetes insipidus, but not the hypoaroused phenotype. *Sci Rep*. 2019; **9**(1): 8243.
35. Eliava M, Melchior M, Knobloch-Bollmann HS et al. A New Population of Parvocellular Oxytocin Neurons Controlling Magnocellular Neuron Activity and Inflammatory Pain Processing. *Neuron*. 2016; **89**(6): 1291-304.
36. Wang L, Goebel-Stengel M, Stengel A, Wu SV, Ohning G, Tache Y. Comparison of CRF-immunoreactive neurons distribution in mouse and rat brains and selective induction of Fos in rat hypothalamic CRF neurons by abdominal surgery. *Brain Res*. 2011; **1415**34-46.
37. Hetz C, Saxena S. ER stress and the unfolded protein response in neurodegeneration. *Nat Rev Neurol*. 2017; **13**(8): 477-91.
38. Luo S, Mao C, Lee B, Lee AS. GRP78/BiP is required for cell proliferation and protecting the inner cell mass from apoptosis during early mouse embryonic development. *Mol Cell Biol*. 2006; **26**(15): 5688-97.

584 39. Ji C, Kaplowitz N, Lau MY, Kao E, Petrovic LM, Lee AS. Liver-specific loss of glucose-
585 regulated protein 78 perturbs the unfolded protein response and exacerbates a spectrum of liver
586 diseases in mice. *Hepatology*. 2011; **54**(1): 229-39.
587 40. Wang X, Bi X, Zhang G et al. Glucose-regulated protein 78 is essential for cardiac myocyte
588 survival. *Cell Death Differ*. 2018; **25**(12): 2181-94.
589 41. Flodby P, Li C, Liu Y et al. The 78-kD Glucose-Regulated Protein Regulates Endoplasmic
590 Reticulum Homeostasis and Distal Epithelial Cell Survival during Lung Development. *Am J Respir*
591 *Cell Mol Biol*. 2016; **55**(1): 135-49.
592 42. Borok Z, Horie M, Flodby P et al. Loss in Epithelial Progenitors Reveals an Age-linked Role
593 for Endoplasmic Reticulum Stress in Pulmonary Fibrosis. *Am J Respir Crit Care Med*. 2020; **201**(2):
594 198-211.
595 43. Wey S, Luo B, Lee AS. Acute inducible ablation of GRP78 reveals its role in hematopoietic
596 stem cell survival, lymphogenesis and regulation of stress signaling. *PLoS One*. 2012; **7**(6): e39047.
597 44. Wang M, Ye R, Barron E et al. Essential role of the unfolded protein response regulator
598 GRP78/BiP in protection from neuronal apoptosis. *Cell Death Differ*. 2010; **17**(3): 488-98.
599 45. Hussien Y, Podojil JR, Robinson AP, Lee AS, Miller SD, Popko B. ER Chaperone BiP/GRP78
600 Is Required for Myelinating Cell Survival and Provides Protection during Experimental Autoimmune
601 Encephalomyelitis. *J Neurosci*. 2015; **35**(48): 15921-33.
602 46. Zhu G, Lee AS. Role of the unfolded protein response, GRP78 and GRP94 in organ
603 homeostasis. *J Cell Physiol*. 2015; **230**(7): 1413-20.
604 47. Grinevich V, Ma XM, Herman JP, Jezova D, Akmayev I, Aguilera G. Effect of repeated
605 lipopolysaccharide administration on tissue cytokine expression and hypothalamic-pituitary-adrenal
606 axis activity in rats. *J Neuroendocrinol*. 2001; **13**(8): 711-23.
607 48. Grinevich V, Ma XM, Verbalis J, Aguilera G. Hypothalamic pituitary adrenal axis and
608 hypothalamic-neurohypophyseal responsiveness in water-deprived rats. *Exp Neurol*. 2001; **171**(2):
609 329-41.
610 49. Itoi K, Jiang YQ, Iwasaki Y, Watson SJ. Regulatory mechanisms of corticotropin-releasing
611 hormone and vasopressin gene expression in the hypothalamus. *J Neuroendocrinol*. 2004; **16**(4): 348-
612 55.
613 50. Grinevich V, Ma XM, Jirikowski G, Verbalis J, Aguilera G. Lipopolysaccharide endotoxin
614 potentiates the effect of osmotic stimulation on vasopressin synthesis and secretion in the rat
615 hypothalamus. *J Neuroendocrinol*. 2003; **15**(2): 141-9.
616

Figure 1

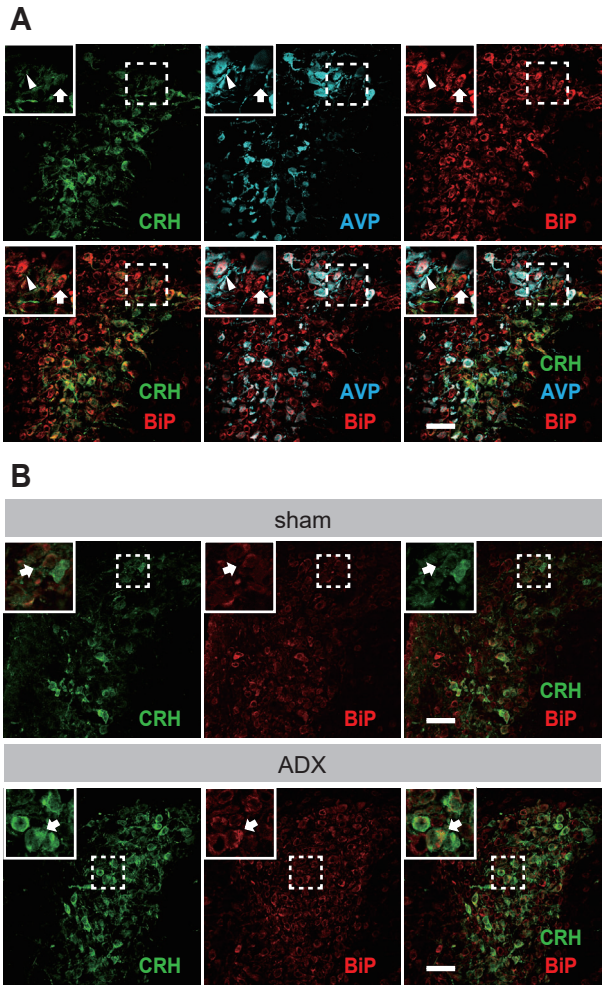
A
CRH
AVP
BiP
CRH
BiP
AVP
BiP
CRH
AVP
BiP
B
sham
CRH
BiP
CRH
BiP
ADX
CRH
BiP
CRH
BiP
C
CRH intensity per CRH neuron (arbitrary units)
200
150
100
50
0
P < .05
sham
ADX
BiP intensity per CRH neuron (arbitrary units)
150
100
50
0
P < .05
sham
ADX
D
Crh mRNA expression (arbitrary units)
400
300
200
100
0
P < .05
sham
ADX
Bip mRNA expression (arbitrary units)
200
150
100
50
0
P < .05
sham
ADX

Figure 2

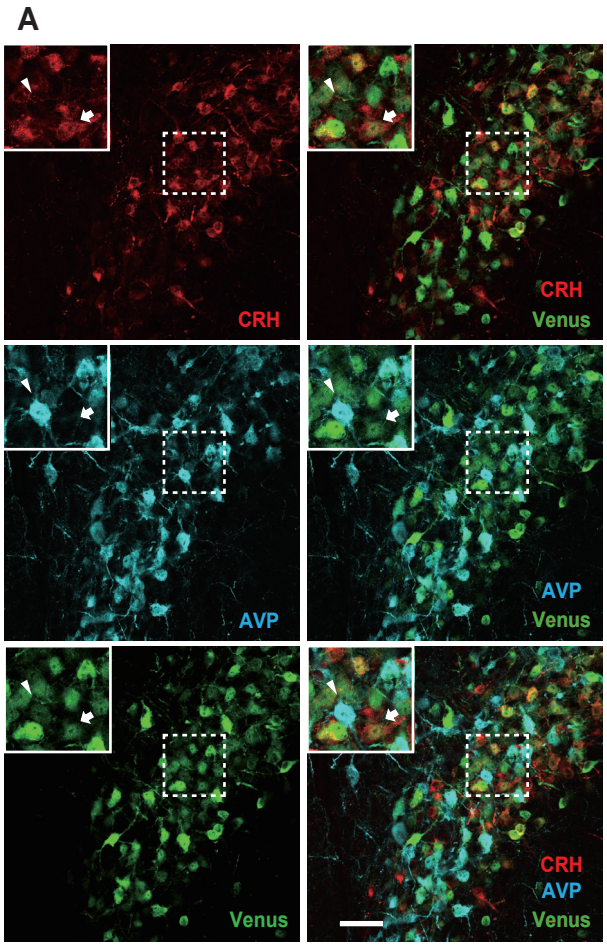
A
CRH
CRH
Venus
AVP
AVP
Venus
Venus
CRH
AVP
Venus

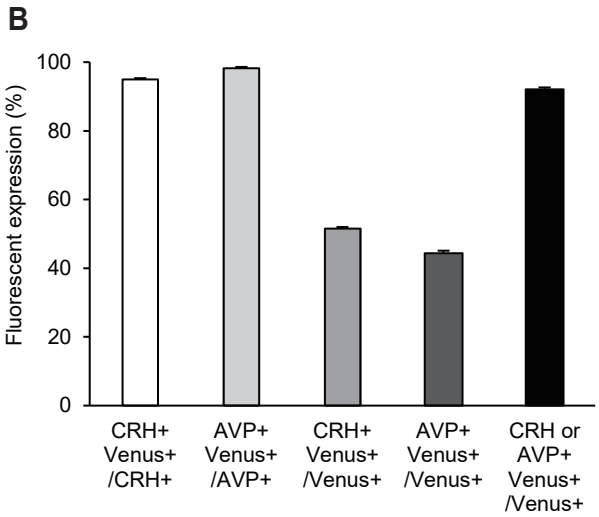
B
Fluorescent expression (%)
100
80
60
40
20
0
CRH+ Venus+ /CRH+
AVP+ Venus+ /AVP+
CRH+ Venus+ /Venus+
AVP+ Venus+ /Venus+
CRH or AVP+ Venus+ /Venus+

Figure 3

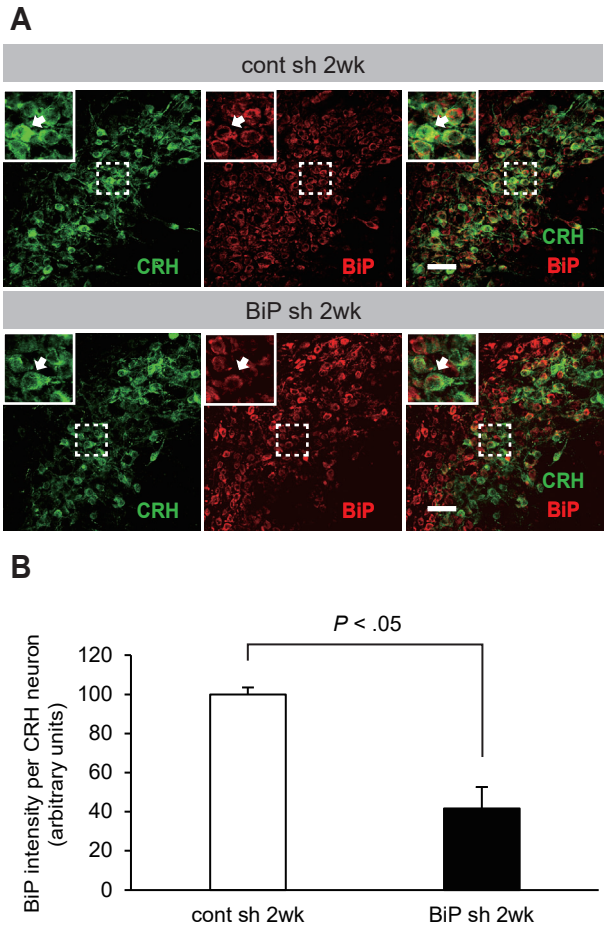
A
cont sh 2wk
CRH
BiP
CRH
BiP
BiP sh 2wk
CRH
BiP
CRH
BiP
B
P < .05
BiP intensity per CRH neuron (arbitrary units)
120
100
80
60
40
20
0
cont sh 2wk
BiP sh 2wk

Figure 4

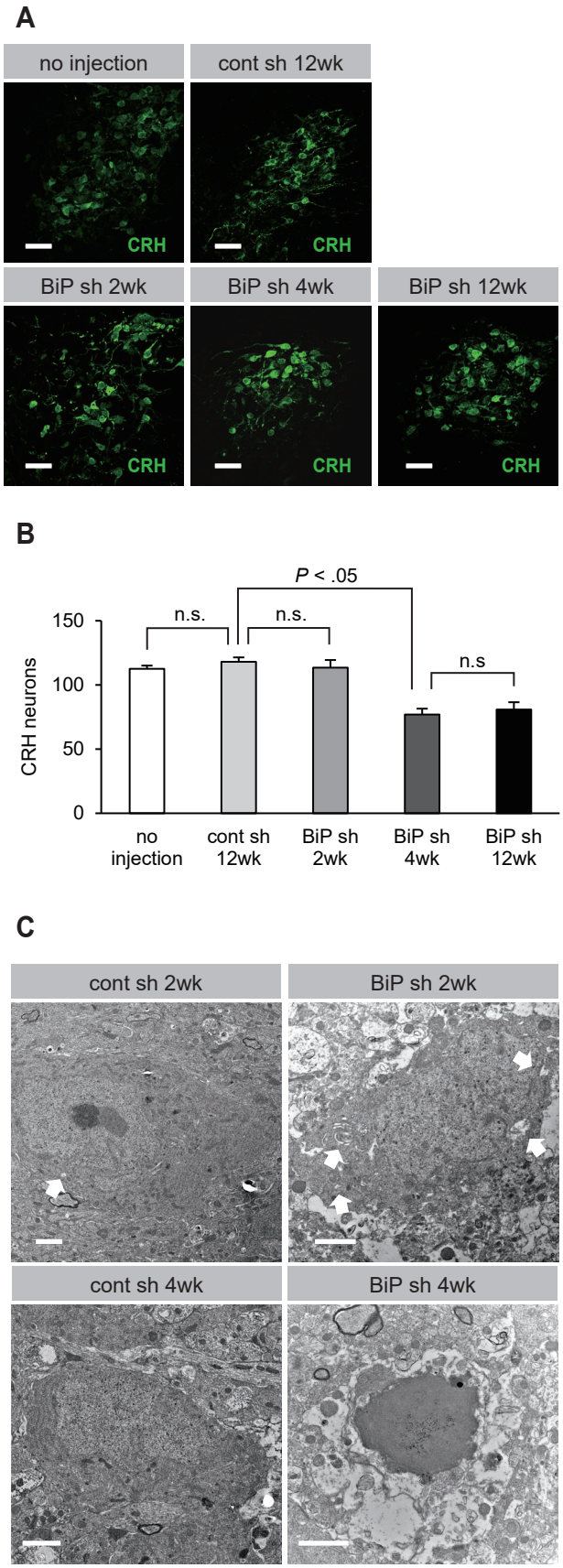
A
no injection
cont sh 12wk
BiP sh 2wk
BiP sh 4wk
BiP sh 12wk
CRH
B
P < .05
n.s.
n.s.
n.s
CRH neurons
150
100
50
0
no injection
cont sh 12wk
BiP sh 2wk
BiP sh 4wk
BiP sh 12wk
C
cont sh 2wk
BiP sh 2wk
cont sh 4wk
BiP sh 4wk

Figure 5

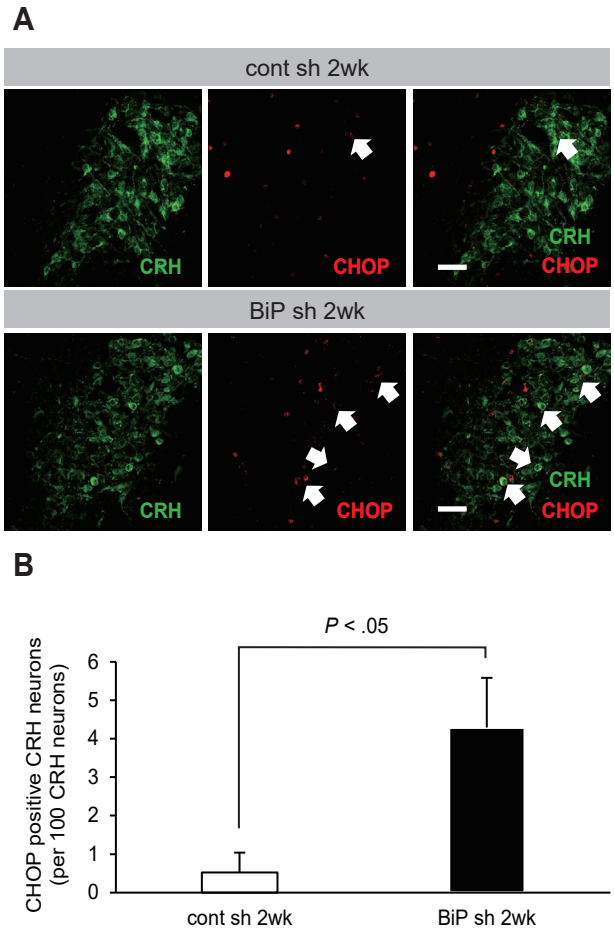
A
cont sh 2wk
CRH
CHOP
CRH
CHOP
BiP sh 2wk
CRH
CHOP
CRH
CHOP
B
P < .05
CHOP positive CRH neurons
(per 100 CRH neurons)
0
1
2
3
4
5
6
cont sh 2wk
BiP sh 2wk

Figure S1

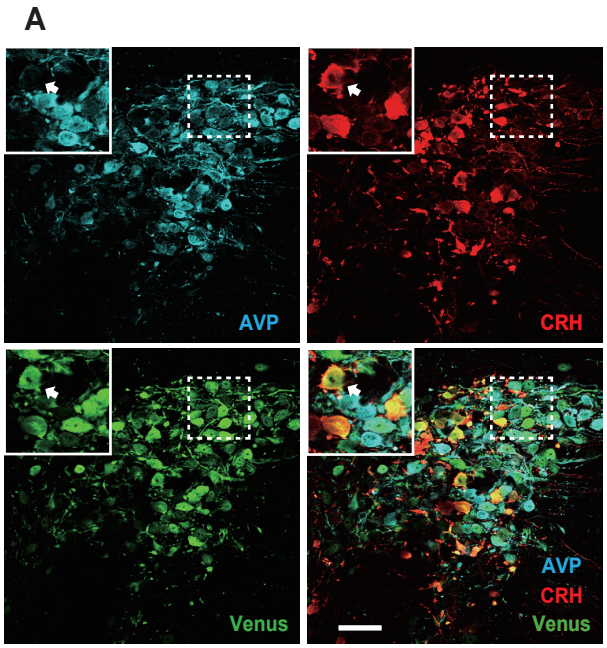
A
AVP
CRH
Venus
AVP
CRH
Venus

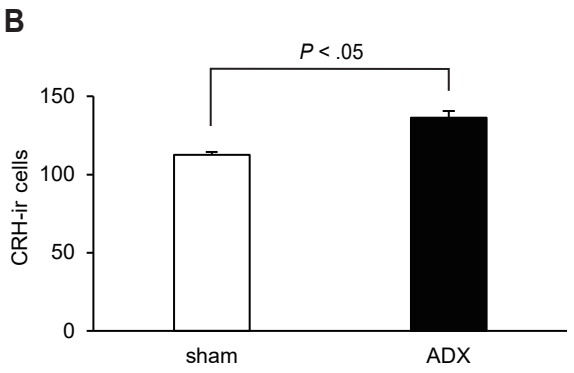
B
P < .05
150
100
50
0
CRH-ir cells
sham
ADX

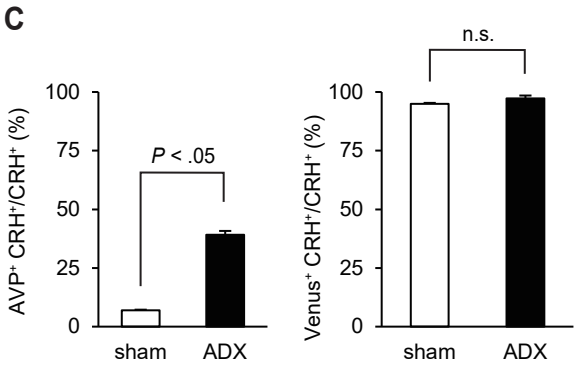
C
P < .05
100
75
50
25
0
AVP+ CRH+/CRH+ (%)
sham
ADX
n.s.
100
75
50
25
0
Venus+ CRH+/CRH+ (%)
sham
ADX

Figure S2

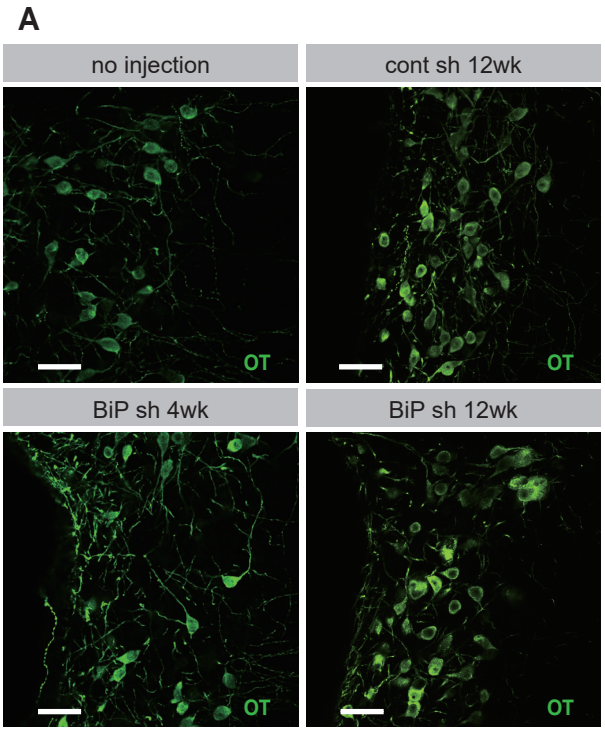
A
no injection
cont sh 12wk
BiP sh 4wk
BiP sh 12wk
OT
OT
OT
OT

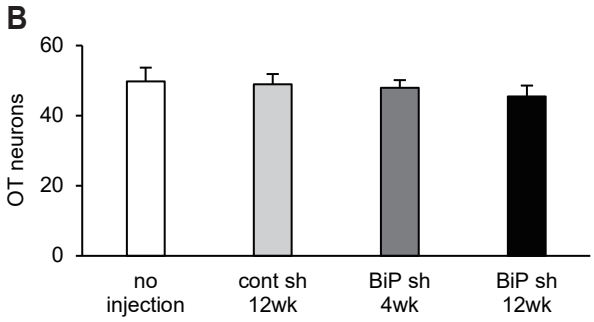
B
OT neurons
60
40
20
0
no injection
cont sh 12wk
BiP sh 4wk
BiP sh 12wk

Figure S3

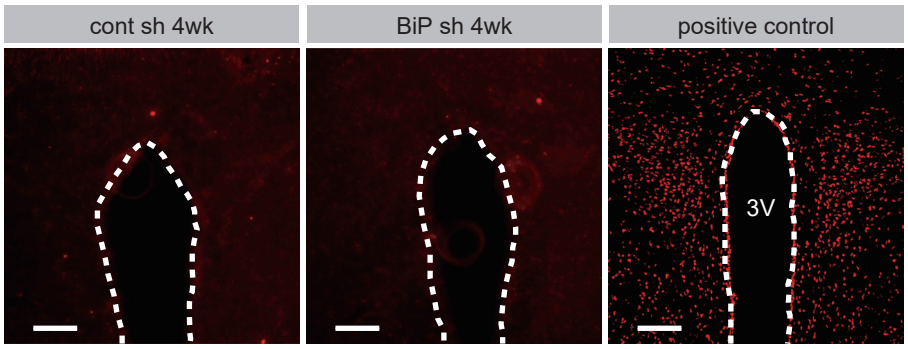

Figure S4

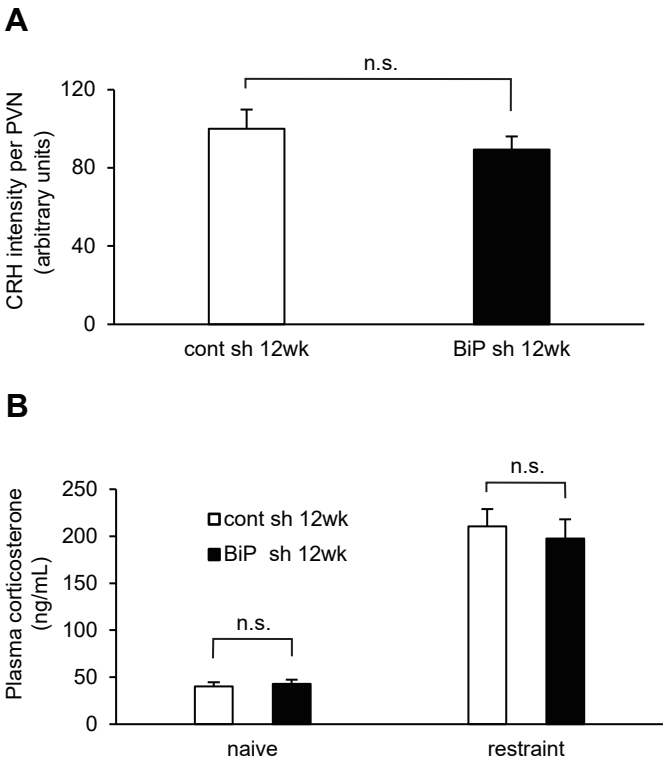
A
n.s.
120
80
40
0
CRH intensity per PVN
(arbitrary units)
cont sh 12wk
BiP sh 12wk
B
n.s.
250
200
150
100
50
0
Plasma corticosterone
(ng/mL)
cont sh 12wk
BiP sh 12wk
n.s.
naive
restraint

Figure S5

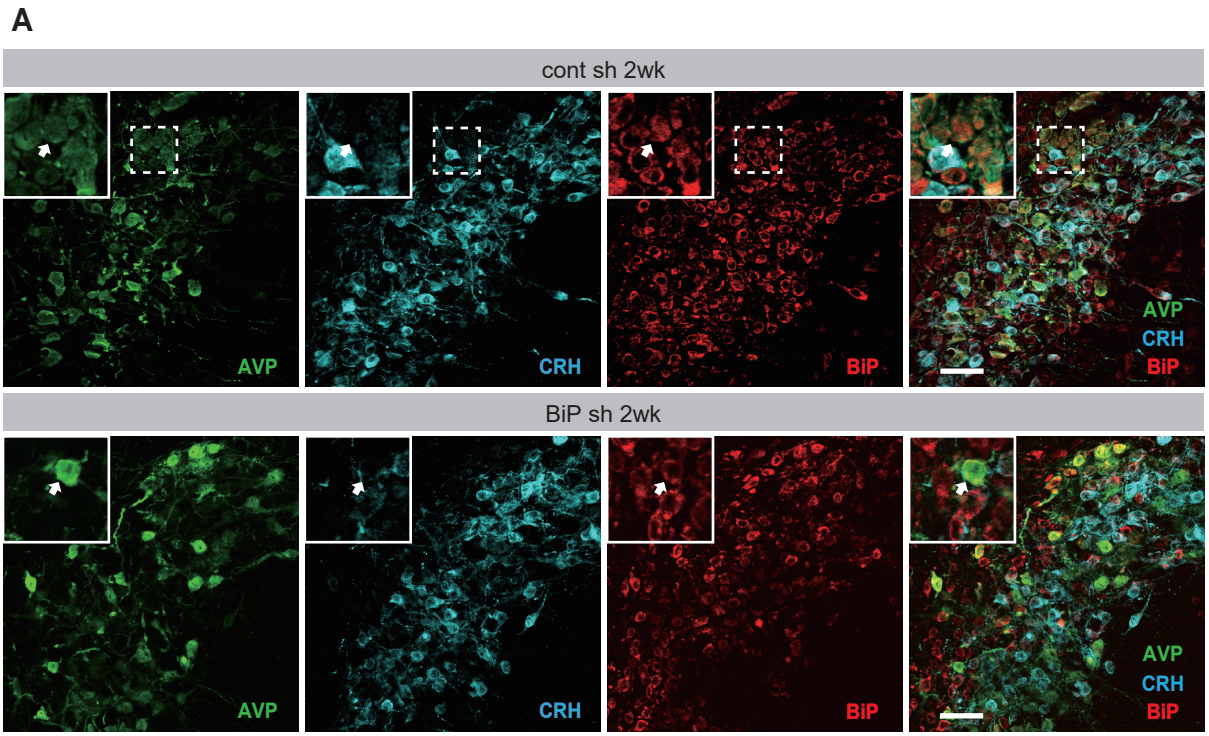
A
cont sh 2wk
AVP
CRH
BiP
AVP
CRH
BiP
BiP sh 2wk
AVP
CRH
BiP
AVP
CRH
BiP

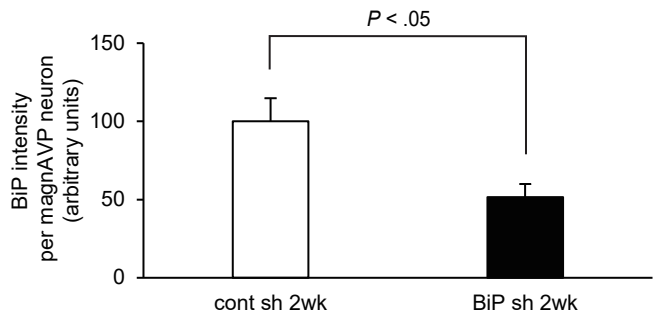
B
P < .05
BiP intensity
per magnAVP neuron
(arbitrary units)
150
100
50
0
cont sh 2wk
BiP sh 2wk

Figure S6

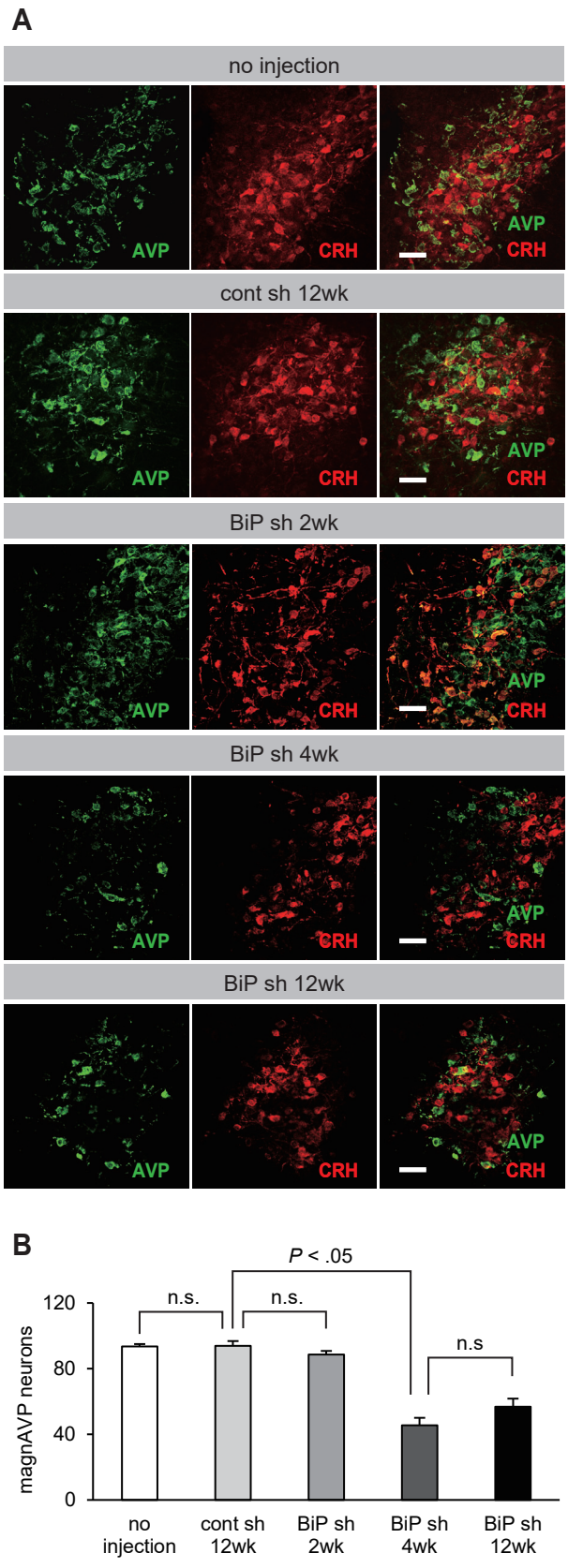
A
no injection
AVP
CRH
AVP
CRH
cont sh 12wk
AVP
CRH
AVP
CRH
BiP sh 2wk
AVP
CRH
AVP
CRH
BiP sh 4wk
AVP
CRH
AVP
CRH
BiP sh 12wk
AVP
CRH
AVP
CRH
B
P < .05
n.s.
n.s.
n.s
120
80
40
0
magnAVP neurons
no injection
cont sh 12wk
BiP sh 2wk
BiP sh 4wk
BiP sh 12wk

Figure S7

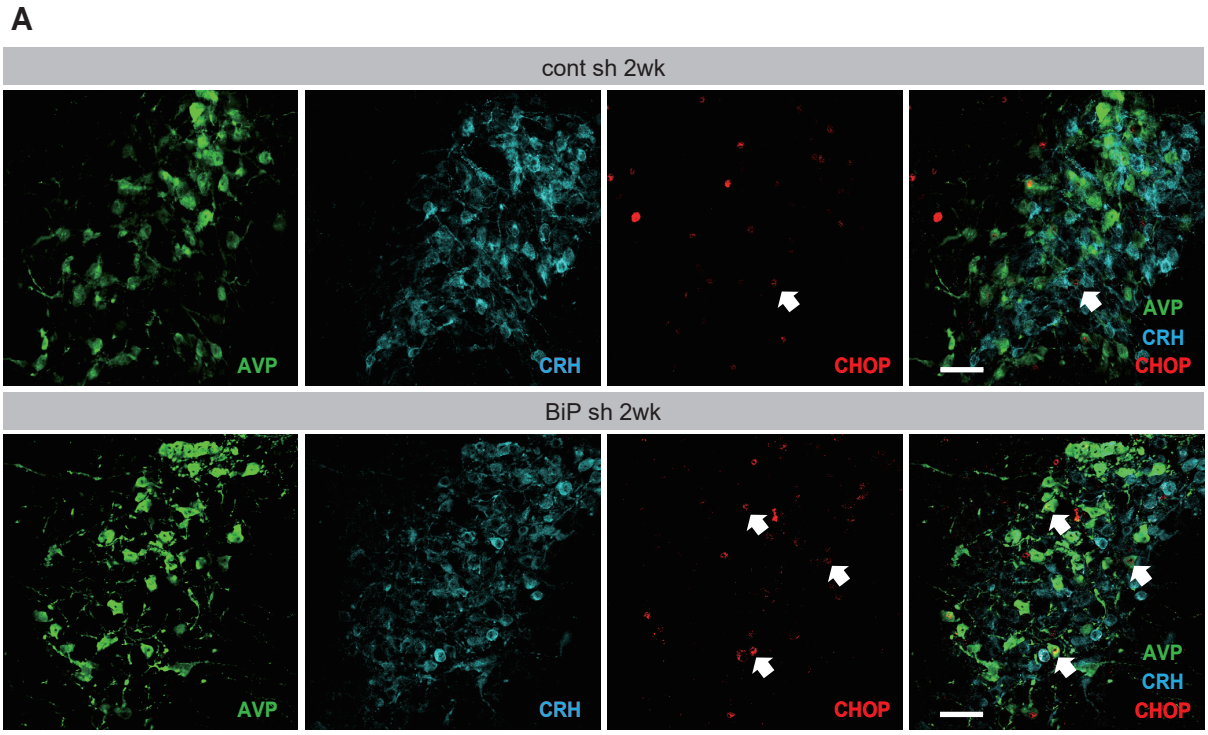
A
cont sh 2wk
AVP
CRH
CHOP
AVP
CRH
CHOP
BiP sh 2wk
AVP
CRH
CHOP
AVP
CRH
CHOP

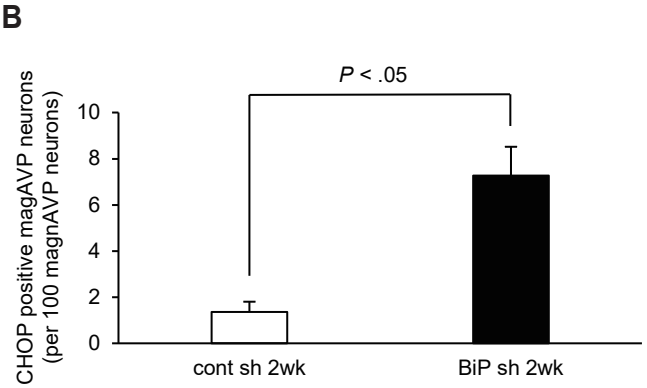
B
P < .05
CHOP positive magAVP neurons
(per 100 magnAVP neurons)
10
8
6
4
2
0
cont sh 2wk
BiP sh 2wk

Figure S8

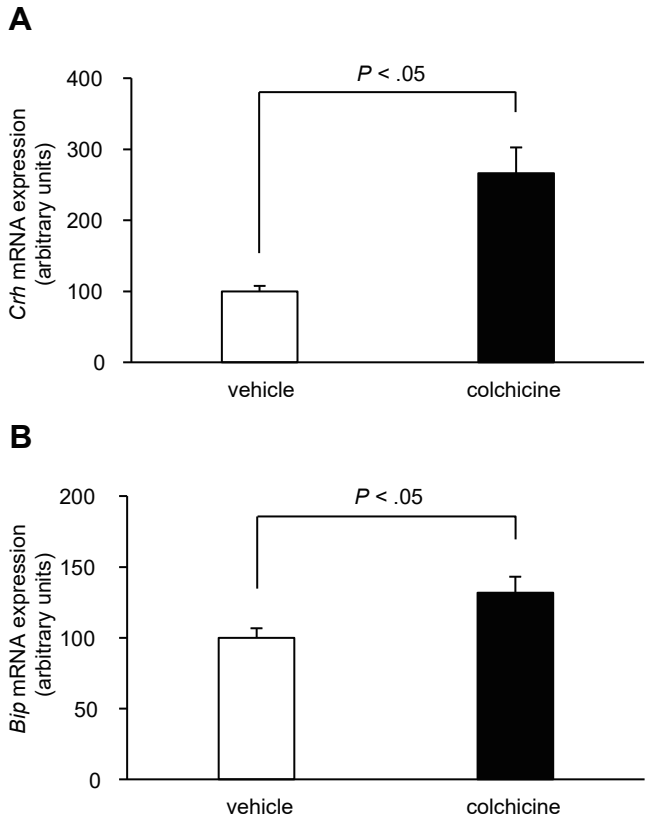
A
P < .05
Crh mRNA expression (arbitrary units)
400
300
200
100
0
vehicle
colchicine
B
P < .05
Bip mRNA expression (arbitrary units)
200
150
100
50
0
vehicle
colchicine